https://doi.org/10.5194/acp-2020-1098
Preprint. Discussion started: 22 October 2020

Atmospheric Chemistry and Physics Discussions

What Drives Daily Precipitation Over Central Amazon? Differences Observed Between Wet and Dry Seasons

Thiago S. Biscaro[1], Luiz A. T. Machado[1,3], Scott E. Giangrande[2], and Michael P. Jensen[2]

[1]National Institute for Space Research, Cachoeira Paulista, São Paulo, 12630000, Brazil.
[2]Environmental and Climate Sciences Department, Brookhaven National Laboratory, Upton, NY, USA.
[3]Multiphase Chemistry Department, Max Planck Institute for Chemistry, 55128 Mainz, Germany

Correspondence to: Thiago S. Biscaro (thiago.biscaro@inpe.br)

Abstract. This study suggests an alternative approach on how diurnal precipitation is modulated by the nighttime events developed over Central Amazon using data from the Observations and Modelling of the Green Ocean Amazon (GoAmazon 2014/5) field campaign in the Central Amazon as well as radar and satellite data. Local observations of cloud occurrences, soil temperature, surface fluxes, and planetary boundary layer characteristics are coupled with satellite data to identify physical mechanisms that control the diurnal rainfall in Amazonas during the wet and dry season. This is accomplished by evaluating the atmospheric properties during the nocturnal periods from the days prior to rainfall and non-raining events. Comparisons between non-rainy and rainy transitions are presented for the wet (January to April) and dry (June to September) seasons. The results suggest that wet season diurnal precipitation is modulated mainly by night-time cloud coverage and local effects such as heat- induced turbulence, while dry season rain events are mainly controlled by large-meso scale circulation.

1 Introduction

As a key component of the atmospheric system, convective cloud processes and their inadequate representations over tropical regions introduce significant uncertainty in numerical weather and climate model predictions (Betts and Jakob, 2002; Dai, 2006). The tropical diurnal precipitation cycle representation has been studied for decades, using numerical models (Bechtold et al., 2004; Sato et al., 2009; Stratton and Stirling, 2012) and observational techniques (Itterly et al., 2016; Machado et al., 2002; Oliveira et al., 2016). Despite the many years of studies, one can point to several unresolved climate model issues over the tropics, including: a) an incorrect phasing of the precipitation diurnal cycle over land that favors models triggering precipitation too early in the day (Gentine et al., 2013); b) poor positioning and potential doubling of the Intertropical Convergence Zone (Hwang and Frierson, 2013); and c) the underestimation of rainfall over the Amazon forest (Huntingford et al., 2004).

Given its unique tropical location and propensity for deep convective clouds having feedbacks to the global circulation, several scientific campaigns have focused on convective cloud, aerosol transportation, and land-atmosphere process interactions over the Amazon forest (Machado et al., 2014; Martin et al., 2016; Silva Dias et al., 2002; Wendisch et al., 2016). Specific to Amazon basin convective cloud studies, model treatments for shallow convection and cloud transitions to deeper convective modes have been identified as a continuing challenge for the correct representation of the diurnal cycle in GCMs (Khairoutdinov and Randall, 2006). Since convection is parameterized in GCMs with convective cloud scales ranging from smaller to larger than the typical GCM grid resolution, the differences in the convective scale driven by the large-scale circulation should be considered in convection parametrization schemes and satellite-based rainfall retrievals (Rickenbach et al., 2002). Moreover, the dynamical, microphysical, and environmental differences between the organized (i.e., larger areal coverage cloud regimes, including Mesoscale Convective Systems; Houze 2018) and/or isolated convective cloud regimes (Schiro and Neelin, 2018) need to be better understood for a correct representation of convective processes.

https://doi.org/10.5194/acp-2020-1098
Preprint. Discussion started: 22 October 2020

Atmospheric Chemistry and Physics Discussions

Recently, the Observations and Modelling of the Green Ocean Amazon (GoAmazon2014/5) campaign (Martin et al., 2016) concluded a two-year deployment over Manaus, Brazil and its surroundings, including an advanced complement of cloud and precipitation profiling instruments. This unique deployment enabled an unprecedented new investigation of cloud lifecycle and associated environmental controls sampled prior to cloud initiation and during subsequent cloud development stages, as well as the associated cloud and precipitation properties. The purpose of this study is to compare environmental conditions observed within the diurnal rainfall cycle in Amazonas and contrasting wet and dry season variability. Specifically, these efforts emphasize changes in the atmospheric conditions and cloud properties observed during the nocturnal periods from days prior to events having no rainfall, and those with rainfall. One motivation for these efforts is to establish potential physical mechanisms responsible for these contrasts between rainy and non-rainy days. These analyses consider conditions over multiple scales by comparing local convection and column observations versus mesoscale cloud properties. This paper is structured as follows: section 2 presents the data used, section 3 defines the transition approach of our methodology, section 4 presents the results, while the conclusions are shown in section 5.

2 Data

The GoAmazon2014/5 field campaign was conducted between January 2014 and December of 2015. The main site (herein, T3) was located in Manacapuru, state of Amazonas (3.213ºS, 60.598ºW), which is roughly 70 km west of Manaus. A comprehensive suite of instruments to measure cloud, precipitation, aerosol and atmospheric state was deployed at T3 as part of the U.S. Department of Energy Atmospheric Radiation Measurement (ARM; Ackerman and Stokes, 2003; Mather and Voyles, 2013) Mobile Facility 1 (AMF1; Miller et al. 2016) during GoAmazon2014/5. Additional details on the AMF deployment and its dataset collection including an overview of cloud coverage and radiative properties, as well as campaign thermodynamic conditions, are provided by Giangrande et al., (2017).

The primary ARM data source for this study is the Active Remote Sensing of CLouds (ARSCLs) Value-Added Product. This data product combines measurements from a ceilometer, a micro pulse lidar, and a vertically pointing W-Band (94 GHz) radar (ARM, 2014). We use the cloud mask available in the ARSCL product to derive profiles of cloud frequency of occurrence. These cloud frequency values were calculated by averaging the occurrences observed over our periods of observation and for the cloud transitions modes as defined in section 3. Similarly, we draw from the ARM Eddy Correlation Flux Measurement System (ECOR) (ARM, 2013a) observations that are used to derive the turbulent kinetic energy and latent and sensible heat fluxes. The T3 site also included a Surface Energy Balance System (SEBS) (ARM, 2013c), used to compute the soil temperature, and a radiometer used to derive longwave irradiances. Finally, GoAmazon2014/15 included frequent radiosonde (ARM, 1993) launches (4 times a day, at fixed 0, 6, 12, and 18 GMT) that are used to estimate convective indices, Convective Available Potential Energy (CAPE) and Convective Inhibition (CIN) (Jensen et al., 2015). Finally, a ceilometer-based approach is used to derive the estimates for the Planetary Boundary Layer (PBL) height (ARM, 2013b).

Rainfall observations are collected by an automatic weather station, with additional support from a nearby surveillance radar to identify rainfall in the vicinity of the site. The nearby SIPAM (Amazonian Protection System) S-Band (2.2 GHz) radar is a single polarization, Doppler weather radar that performs a volume scan each 12 minutes, with a 2° beam width and radial resolution of 500 m. The SIPAM radar is located in Manaus and has a 240 km radius range. For spatial cloud field property analysis, the GOES 10.4 μm brightness temperature data acquired over a 10° x 10° box centered on T3 were used to verify the occurrence of cold cloud tops that would indicate the presence of precipitating clouds around the studied region. GOES data were received and processed operationally by CPTEC/INPE (Centre for Weather Forecasting and Climate Research/National Institute for Space Research) (Costa et al., 2018).

https://doi.org/10.5194/acp-2020-1098
Preprint. Discussion started: 22 October 2020

Atmospheric Chemistry and Physics Discussions

3 Classification of Raining and Non-Raining Events

In the Amazon, convection typically initiates around noon and precipitation presents its maxima around 14 LT (Machado et al., 2002). We define a previous day 'nocturnal period' as the period between 00 GMT and 12 GMT (20 LT to 08 LT), and the following 'diurnal period' as the period between 12 GMT and 00GMT (08 LT to 20 LT). The diurnal period starts roughly 2 hours after the sunrise in Manacapuru, which occurs around 06 LT and does not vary much throughout the year. To understand what controls the convection for the daytime period that follows, we categorize Amazon observations into two classes: a) days having no rain during the nocturnal period and no rain during the subsequent diurnal period; and b) days having no rain during the nocturnal period, but observing rain during this subsequent diurnal period. We refer to these transitions as NR-NR (No Rain to No Rain) and NR-RR (No Rain to Rain), which comprise separate 24-hour events. Our intention is to identify the possible controls during nocturnal periods that may initiate precipitation in the subsequent diurnal window. For completeness, days recording rain within the nocturnal period (39% of the days during the wet season, and 9% during the dry season) are not considered for this analysis, as we are only interested in diurnal cloud cycling and the onset of precipitation. The choice of a 12-hour nocturnal period having no precipitation also provides an additional control, since daytime convection having precipitation is frequent, and especially during the wet season. Thus, we do not assume that convection is only dependent on nocturnal conditions but expanding such periods to a full (prior) day conditions would often result in precipitation observations.

We used local weather station datasets at T3 as well as gridded SIPAM radar datasets (1 km-horizontally gridded, 3 km-level constant altitude plan position indicator (CAPPI))) to define precipitation events. The SIPAM monitoring of the area was done to include days where local/column observations would otherwise miss reasonable rainfall events. A 50 x 50 km area (similar to a typical GCM gridbox resolution) centered at the T3 site was used, and gridded radar reflectivity factor values greater than 25 dBZ in this domain were considered as 'precipitation' echoes. If more than 10% of the area was covered by such reflectivity values greater than 25 dBZ at any time during any given hour, or if the local weather station reported a rainfall accumulation greater than 1 mm during that same hour, then we defined the day as a rain (NR-RR) event.

For this study, we defined the 'wet' season as the period between January and April and the 'dry' season as between June and September (Giangrande et al., 2017, Machado et al., 2018). To ensure sufficient sampling, we used the entire GoAmazon2014/5 record (2014 and 2015) in our analysis and did not attempt to differentiate year-to-year GoAmazon2014/5 dataset variability, such as the case in previous Amazon efforts (e.g., Jiménez-Muñoz et al., 2016). Following our definitions, we identified 51 NR-NR cases and 113 NR-RR cases during the wet season. The dry season showed a reversal in event frequency, with 148 NR-NR cases and 64 NR-RR cases. These cases were distributed throughout the campaign as presented in Figure 1. No intra-seasonal variability is observed in those distributions, however an ENSO event of 2015 is pronounced (e.g., Jiménez-Muñoz et al., 2016), as suggested by the larger number of NR-NR cases during the dry season of 2015 (Figure 1 (d)). Also, NR-RR days with an active Kelvin wave mode were only found for 7% of this wet season dataset (not shown, a classification of Kelvin wave activity was kindly provided by Dr. Yolande Serra from the Joint Institute for the Study of the Atmosphere and Ocean – University of Washington).

Possible river-breeze or other land contrasts influences in the rainfall distribution are expected, but they are not object of this study. Land-breeze effects are known to enhance the nocturnal rainfall in near-river areas (Cohen et al., 2014; Fitzjarrald et al., 2008) and affect local low-level circulation in near-river areas (de Oliveira and Fitzjarrald, 1993). All of our data was obtained over the same site (T3), located 10 km from the Solimoes and 25 km from the Negro river. The site and its surrounding did not suffer any deforestation or change in its surface coverage over the 2 year period of our analysis. Furthermore, radar analysis provided by Dr. Die Wang from the Brookhaven National Laboratory shown that precipitation is enhanced southwest from the SIPAM radar, regardless of river proximity. Therefore, we define "local influences" here as influences within a few kilometers around the site, occurring in this area between the rivers, which could be represented in a typical GCM grid.

https://doi.org/10.5194/acp-2020-1098
Preprint. Discussion started: 22 October 2020

Atmospheric Chemistry and Physics Discussions

4 Results

4.1 Results from local observations

4.1.1 Low cloud diurnal cycle from cloud radar

In Figure 2, we display ARSCL-derived mean cloud fraction values. This represents the average fraction of time when a cloud was observed over the site during each observation period, and for the various rain regime separations (i.e., pairings for wet/dry season breakdowns, and NR-NR/NR-RR modes). Initial emphasis is on the lower portion of the atmosphere below the freezing level (approximately 4.5 km) since we anticipate shallow clouds during non-raining nocturnal periods. Note, residual cirrus from the previous day deeper cumulus clouds (or advected into the domain from distance) may be anticipated, however these upper level clouds are not the focus of this analysis. In the bottom panels of Figure 2, we plot the absolute cloud occurrence difference between the modes for the wet and dry seasons, respectively. The local time axes on these images has been extended to 12 LT to better illustrate the onset of convection (or lack thereof) in our mode and difference properties.

Consulting wet season properties along the leftmost panels, one can note that the NR-NR transition (Figure 2 (a)) presents higher cloud coverage during the night than the NR-RR mode (Figure 2 (b)). The NR-NR mode features cloud occurrences above 20% from 22 LT to 04 LT between 1 and 3 km, and from 00 LT and 04LT in several cases. In addition, the NR-NR mode suggests an earlier onset for shallow clouds than the NR-RR transition days, and the near-surface occurrences are higher than 20% most of the times from 00 LT to 04 LT. These near surface shallow clouds may be attributed to fog, frequently observed from midnight to noon during the wet season (Anber et al., 2015, Giangrande et al., 2020). From sunrise until 10 LT, the NR-RR mode also suggests low-level cloud activity, possibly related to fog occurrence as well. During the late morning, the NR-NR mode indicates a high frequency of shallow convection after 10 LT, with cloud occurrences exceeding 45% confined to a shallow layer around 1 km altitude. During the raining transition the 1 km-layer cloud coverage is generally lower compared to the NR-NR mode, where before 06 LT cloud occurrence rarely exceeds 15%. The shallow convective activity observed at sunrise is weaker than the wet NR-NR mode, but after 10 LT cloud occurrence exceeds 45% and its 30% contour height reaches 2.5 km. Note, since we extend our period of study from 08 LT to 12 LT, there will be raining clouds contaminating these results after 08 LT, for all transition modes and seasons. The absolute difference (Figure 2 (c)) shows that for most times from 22 LT to 04 LT, the non-raining mode has higher cloud occurrence, especially below 6 km, with differences around 20%, which happens also frequently in higher levels between 20 LT and 22 LT. After 10 LT the NR-RR mode shows the maximum negative cloud differences, reaching -20%.

A physical interpretation of the wet season results is that this higher cloud occurrence in the NR-NR mode during the nocturnal periods would imply additional consumption of energy that might have been available for convection during the following daytime period. One question is whether these night-time clouds could be formed by radiative cooling from the top of the boundary layer, thus not associated with consumption of CAPE. However, CAPE and CIN observations (subsequent section) indicate these thermodynamic parameters are reduced for these NR-NR modes. In addition, cloud coverage during early mornings (frequency over 25% observed between 06 and 07 LT near the surface and at 3 km AGL) would limit surface heating, e.g., reduced incoming solar radiation. Alternatively, an increase in the incidence of solar radiation during the NR-RR mode associated with reduced cloud coverage generates surface heating that would favor subsequent daytime convective development. This behavior was discussed from an energy budget standpoint by Machado (2000), where it was shown that the surface loses more energy than it receives in convective events, therefore reduced energy is available at the surface following a cloudy period. Using observations over the Amazon, they show that the surface

https://doi.org/10.5194/acp-2020-1098
Preprint. Discussion started: 22 October 2020

Atmospheric Chemistry and Physics Discussions

absorption of solar energy was always smaller (larger) than the total surface flux provided to the atmosphere throughout convective (non-convective) events. The quantity of energy stored at the surface seemed to be constrained, and defines a timescale, during which the surface needs to export or receive energy to stabilize its deficit or gain of energy. Beginning at 06 LT the differences throughout the whole column (except close to surface between 06 and 07 LT) favor the NR-RR mode.

The dry season results illustrate most of the cloud activity during the night-time window occurs at the higher cloud levels (i.e., above 7 km, and provides a strong contrast with the increased lower cloud coverage observed during the wet season (e.g., between 0 and 6 km). The NR-NR mode (Figure 2 (d)) suggests reduced cloud occurrence (e.g., frequency values less than 15%) during the night-time hours. The NR-RR cases (Figure 2 (e)) suggest increasing cloud coverage above 1 km and additional near-surface/low clouds after 08 LT, which contrasts with the NR-NR modes that suggest low-cloud occurrence below 5%. The difference field for the dry season (Figure 2 (f)) implies that the raining mode is predominantly cloudier than the NR-NR mode. During the nocturnal period, the maximum difference in occurrence falls between an 8% to 12% increase in the favor of the NR-RR mode (here, for the levels between 2 and 4 km). Thus, these dry season non-rain to rainy differences are reduced (in absolute value) when compared to the wet season behaviors. A physical interpretation for these dry season behaviors will be discussed in section 4.2.

4.1.2 Radiosonde analysis

In Figure 3, we present statistics for the thermodynamic parameters CAPE and CIN using data derived from the nocturnal (20, 02, and 08 LT) radiosondes launched at T3. The boxplots were constructed to display the minimum, lower quartile, median, upper quartile, and maximum values.

As previously introduced, the wet season CAPE results (Figure 3 (a)) suggest a reduction of the potential energy from 20 to 02 LT during the NR-NR transition (grey boxes), whereas the NR-RR mode results (blue boxes) are similar for these two measurements. Recall, a physical explanation for this reduction in CAPE between the two first observations (20 and 02 LT) is convective cloud energy consumption, since a cloudier condition is argued between 22 and 02 LT for these NR-NR transition events. The NR-NR 20 LT CAPE is the highest magnitude/distribution we observe, suggestive for an eventual increase of the cloud coverage, which in turn consumes this energy, but ultimately decreasing the CAPE by the measurements of the subsequent sounding. Between 02 and 08 LT, we observe an increase in the distributions for CAPE for NR-NR and NR-RR modes during the wet season. This increase is suggested as owing to the surface heating and the increase of the surface temperature after the sunrise. CAPE values are observed higher for the NR-RR mode by the timing of the 02 LT and morning 08 LT radiosondes when contrasted with the NR-NR mode composites. By 20 LT (typically, after daytime rainfall onset), the non-raining mode still indicates the largest upper quartile value and maximum CAPE values, albeit the medians are nearly identical between NR-RR and NR-RR modes.

The dry season (Figure 3 (b)) plots indicate higher CAPE values at the morning 08 LT radiosonde times when compared to the wet season for each mode we present. These results are compatible with the higher soil temperature (and overall reduced precipitation, surface moisture) observed during the dry season. The energy decrease in the NR-NR mode between 20 and 02 LT is present, yet less pronounced than that observed during the wet season. The NR-RR changes observed between 20 and 02 LT are subtle: a slight increase of the upper quartile value and a decrease of the maximum value. An explanation for the similarities between the 20 and 02 LT results, for both modes, and their differences in comparison with the wet season results, is the reduced cloud coverage (overall). Moreover, reduced or less favorable cloud coverage, as observed during the dry season, implies a lower convective activity overall. The 02 LT sounding values are similar for the dry and wet seasons, for both NR-NR and NR-RR transitions. The wet season CIN (Figure 3 (c)) shows that the convective inhibition is less intense than those observed during the dry season (Figure 3 (d)), for all times and transitions. For both seasons the largest inhibitions are displayed during the 02 LT sounding, for the NR-NR mode.

https://doi.org/10.5194/acp-2020-1098
Preprint. Discussion started: 22 October 2020

Atmospheric Chemistry and Physics Discussions

Finally, a t-Student test was applied to this dataset. These efforts found that the differences between the modes were significant at the 0.05 level for the 02 and 08 LT results above. However, the 20 LT observations were not found to meet these significance criteria. These statements include both the CAPE and CIN behaviors, and the behaviors for wet and dry seasons. Overall, these results may be somewhat expected, but these properties are presented to demonstrate a strong consistency with behaviors discussed for the NR-NR versus NR-RR modes.

The composite radiosondes are presented in Figure 4 (02 LT composite) and Figure 5 (08 LT composite). Left panels indicate wet season observations, solid lines are NR-RR data, and dashed lines are NR-NR data. As one might expect, the dry season composites are much drier than their wet season. One feature that can be noticed in these composites is higher temperatures close to the surface in the 02 LT data than those observed in the 08 LT sounding, corroborating with the surface temperature observations (not shown) that presented higher temperatures from 02 LT up to 08 LT. The dry temperature profiles present subtle differences between NR-RR and NR-NR modes during the dry season, and they are almost the same for the wet season. Rain/no-rain differences in the dew point temperature profiles are more pronounced than those observed in the dry temperature profiles (especially during the dry season). There is evidence that dry season precipitation is linked to larger-scale moisture advection, as we will discuss in section 4.1.5.

4.1.3 Sensible and latent heat fluxes analysis

Cloud coverage directly impacts the incoming solar radiation by changing the Earth-system albedo. A higher (lower) cloud coverage will imply in less (more) incident solar radiation reaching the surface, altering the sensible and latent heat flux balance. As the surface heats up, thermally induced turbulence is produced, via convection. As presented in Figure 2, the wet season NR-RR mode presents lower cloud occurrences up to 1 hour after the sunrise, when the magnitude of both sensible and latent heat fluxes begin to grow. To examine the relationships between cloud coverage and surface fluxes, we present the mean latent heat flux and the mean sensible heat flux measured by the ECOR system, in Figure 6 and Figure 7. Since the ECOR did not operate during the year of 2014, only 2015 data are plotted. As mentioned before, we are not interested in large time-scale variability, so it would be better to study a limited dataset than just displaying a case-study (in contrast to all mean/composites analysis presented) or use reanalysis to compare the NR-NR and NR-RR seasonal behaviors.

During the dry season (Figure 6 and Figure 7, right panels) both fluxes have approximate the same values during both modes, with mean behaviors superimposed most of the times during boundary layer growth. However, in the wet season, the latent and sensible heat fluxes (Figure 6 and Figure 7, left panels) present different characteristics during the NR-NR and NR-RR modes: we observe higher flux values during the NR-RR modes up to 08 LT, and after 08 LT, with the onset of precipitation, temperature drops and the differences between the NR-RR and NR-NR fluxes becomes negative. The fluxes analysis seems to corroborate the local cloud coverage results (Figure 2), since dry season fluxes are statistically the same (when looking at low cloud occurrence differences) and during the wet season the NR-NR fluxes are lower, when we notice more cloud coverage during the NR-NR mode, reducing the incoming solar radiation and therefore surface heating in comparison with the NR-RR mode. This analysis also indicates the role of the surface moisture in the PBL development. The higher soil moisture in the wet season may lower the Bowen ratio, favoring latent heat and developing more clouds, thus lowering the PBL (Giangrande et al., 2020), as we discuss in the next sections.

4.1.4 Planetary boundary layer analysis

The planet boundary layer over the Amazon was subject of study of past field-campaigns, such as the Amazon Boundary-Layer Experiment – ABLE2a and ABLE2b (Harriss et al., 1988; Garstang et al., 1990) and also during the Large Scale Biosphere-Atmosphere Experiment – LBA (Silva Dias et al., 2002). Studies such as Martin et al., 1988, and Fisch et al., 2004, described the characteristics and evolution of the PBL over the Amazon during these experiments. The depth of the mixed layer below cloud base as well as the relative humidity near surface and the lifting condensation level are tightly

https://doi.org/10.5194/acp-2020-1098
Preprint. Discussion started: 22 October 2020

Atmospheric Chemistry and Physics Discussions

coupled in the diurnal convective boundary layer over the Amazon (Betts et al., 2006). The composite dataset planetary boundary layer heights properties for the various modes and seasons as estimated using ceilometer are plotted in Figure 8. As already demonstrated in previous studies (e.g., Betts et al., 2002, 2013), the wet season, being the season with most convective precipitation activity overall, presents lower PBL heights. As from Figure 8, the observed PBL heights during the dry season are higher than the wet season ones, and even the NR-RR mode of the dry season has a higher PBL than the wet season NR-NR mode. During the wet season, the distinction between the NR-NR and NR-RR transitions begins to appear at 08 LT. The maximum PBL height (approximately 1000 m) is reached around local noon for the NR-RR transition, whereas the NR-NR maximum is 500 m higher and reached 2 hours later. Both height and time differences observed can be explained by the more frequent convective development that occurs the wet season. With moisture freely available during the wet season, any conditional instability that favors cloud development such as surface heating or local instabilities can trigger convection, thus lowering the PBL. Carneiro (2018) and Carneiro et al. (2020), using observational data from ceilometer, LIDAR, and LES simulations shown that the erosion of the nocturnal boundary layer occurs 2 hours after the sunrise during the dry season and 3 hours after the sunrise during the wet season.

The normalized hourly rainfall occurrence distribution (Figure 7) suggest that the precipitation occurrences are more distributed over the daytime window during the wet season, while the dry season distribution indicates a distinct peak around noon. In total, 502 events were observed in the wet season and 192 events were observed in the dry season during this GoAmazon2014/5 period. The seasonal differences between the diurnal cycles of the rainfall occurrence may help explain the contrasts observed between the PBL heights. In the dry season, one third of the rainfall occurrences is observed between 12 and 14 LT, which corresponds to the time when the NR-RR and NR-NR PBL heights begin to present a more prominent difference, in contrast with the wet season, where the PBL heights are different from 08 LT.

The ECOR derived turbulent kinetic energy (TKE) results are presented in Figure 10. TKE was measured at 3 m from surface, and although flights were available during the campaign, they were scarce (less than 20 flights per IOP), not allowing us to use the data for a statistical analysis. Results show that the dry season presents higher values of TKE than the wet season with few differences between the modes. However, clear differences between the wet season modes are observed, with the NR-RR mode having the higher values of TKE, reaching 1.2 $m^{-2}s^{-2}$ around the local noon. The NR-NR and NR-RR wet season curves show significantly different values after 10 LT, indicating a more turbulent low-level atmosphere in the presence of rain during the wet season. During the wet season, the raining mode presents higher TKE values overall. Before the onset of convection, this behavior can be related to larger surface heat fluxes (presented in Figures 4 and 5, right panels) from 06 to 09 LT. In the presence of rain, the larger TKE values can be explained by turbulence generated by stronger winds observed during rain cell events. Oppositely, the dry season TKE is similar for both NR-NR and NR-RR modes. The similar magnitudes may be an indication of drier soil conditions, overall absence of shallow clouds, an indication of higher temperatures during both modes, or some combinations therein to be discussed below, but during the wet season the difference is highlighting the importance of local cloud processes in the rainfall events.

Surface temperature also plays an important role on the TKE, since higher surface temperatures will increase thermal turbulence and near-surface wind speed (Jacobson, 2005). On the TKE results (Figure 10), we observe that TKE is lower during the wet season, for both modes, which can be a response to the lower temperatures observed in this period, as we present in Figure 11. The wet season temperatures (Figure 11, left panel) presents higher differences between NR-NR and NR-RR modes beginning at 12 LT, due to surface cooling caused by rainfall beginning at 08 LT. Dry season temperatures (Figure 11, right panel) are similar for both modes, which is an indication that the temperature does not change as much during rain events in comparison with the wet season, and helps explain the similarity between NR-NR and NR-RR dry season TKE curves. Also, in the dry season, one might anticipate a drier soil (resulting in higher Bowen ratios), and a drier boundary layer (less clouds), implying in a stronger generation of turbulent boundary layer growth (Giangrande et al., 2020, Jones and Brusnell, 2009).

https://doi.org/10.5194/acp-2020-1098
Preprint. Discussion started: 22 October 2020

Atmospheric Chemistry and Physics Discussions

290

4.1.5 Local observations – summary

The results presented in the previous sections indicate that the precipitation onset in the dry season is weakly correlated with local factors. However, the local ARM site observations presented – cloud fraction, fluxes, CAPE/CIN, PBL characteristics, surface temperatures, and turbulence – show distinct features between non-raining and raining transitions during the wet
295 season, with CAPE/CIN also showing a significant difference between rain and non-rain modes during the dry season. Also, these features are correlated: soil temperature and TKE presents the same NR-NR/NR-RR difference characteristics, as well as PBL height and rainfall, surface fluxes and cloud coverage. Although the dry season analysis presented similar characteristics between raining and non-rain modes, (Ghate and Kollias, 2016) state that during the dry season local land-atmosphere interactions may trigger the transition from shallow to deeper convection, and indicate a relationship between
300 large-scale moisture advection and precipitation. We did not find evidence for local interactions being responsible for dry season diurnal precipitation, nor we analyzed moisture advection, but we present a large-mesoscale cloud analysis in the next section.

4.2 Large-mesoscale analysis

To further investigate the influences of local effects versus the influence of the mesoscale cloud patterns from the nocturnal
305 period on the subsequent rain transitions, we calculated the mean field of the GOES 10.4 μm brightness temperatures observed over a 10° x 10° box centered at T3 during the nocturnal period. In addition, we calculated the cumulative distribution function (CDF) and the probability distribution function (PDF) of these brightness temperatures, grouped in 3h intervals and separated by transition type and season. Mean brightness temperature fields during the nocturnal period (20 LT – 08 LT) observed over a 10° x 10° box centered at T3 (the cross mark in each panel) are presented in Figure 12. These are
310 shown for NR-NR and NR-RR modes (top and middle panels), and for wet/dry season breakdowns (left and right columns, respectively), with absolute differences presented on the bottom panel. These brightness temperature fields can be related to the cloud occurrence fields from Figure 2, as higher cloud occurrences will result in lower brightness temperature means.

Anticipated differences (as from ARSCL properties in Figure 2) in convective activity between NR-NR and NR-RR transitions during wet and dry seasons are hold in these spatial cloud field representations. For example, convection is more
315 intense during the wet season (Figure 12 (a) and (b)), and it is observed around the whole domain. Temperatures below 275 K can be observed in more than 90% of the region for both transition types. Roughly 81% of the differences between NR-NR and NR-RR modes are statistically non-significative (Figure 12 (c)). The differences among the two transition modes in the wet season is related to the terrain: the regions in the north and southwest of the domain, that presents the main differences, are areas where there the dominant wind flow (from northeast) are lifted over areas where the terrain elevation
320 rises (Figure 13).

During the dry season, the NR-NR transition ((Figure 12 (d)) is associated with warmer temperatures, and values above 280 K comprise almost all the region. The NR-RR transition (Figure 12 (e)) suggests colder temperatures, 5 to 10 K lower than the NR-NR transition overall. Approximately 72% of the temperature differences between the non-raining and raining mode are found between 8 and 20 K (Figure 12 (f)). This feature strongly suggests that the large-scale cloud conditions during the
325 dry season are very different between raining and non-raining days.

The mean behavior observed in Figure 12 can be detailed breaking the observations in fixed time intervals. In Figure 14, we present the PDF of the GOES-13 10.4 μm brightness temperatures grouped into 3 h time steps over the nocturnal period. This breakdown helps diagram the evolution of the convective systems around the T3 site and identify the differences presented between seasons and transitions therein. All distributions plotted in Figure 14 are left-skewed unimodal

https://doi.org/10.5194/acp-2020-1098
Preprint. Discussion started: 22 October 2020

Atmospheric Chemistry and Physics Discussions

distributions, with peaks between 285 K and 295 K. Wet season distributions (dashed lines, both modes) are similar for both transition modes and for all time intervals considered. Values observed for the wet season are generally lower (colder temperatures) than those observed in the dry season, indicating a stronger convective activity throughout the domain independent of transition type or time interval. Dry season distributions (solid lines, both modes) are quite different during NR-NR (black lines) and NR-RR (red lines) events, with a larger incidence of higher values (e.g., warmer temperatures or absence of higher clouds) during NR-NR transitions.

The wet season mean cloud field similarities are better illustrated in the CDFs (Figure 15), where these CDFs indicate that the wet season mean cloud field does not change as much as the dry season distributions during the overnight window, regardless of the precipitation observed during the subsequent day. In other words, the wet season large-meso scale mean convective characteristics have approximate the same characteristics for both transition modes, and the development of precipitating clouds observed at T3 during the wet season appears to be influenced mostly by local factors, as discussed before. In contrast, the dry season distributions (solid lines) are quite different: the lower quartile (Q1) value of the NR-RR transitions (red lines) is often reached around 250 K, while for the NR-NR transitions (black lines) the Q1 value lies around 280 K. The NR-NR CDFs are very similar for all time intervals, but the NR-RR CDFs change with the time, and the differences between them increases as time passes. The dry season NR-RR curves also suggest colder values than the wet season curves from 23 LT onwards, which implies that when precipitating convection happens during the dry season, these clouds tends to be stronger/deeper than those in the wet season. This finding for intense dry season convection is consistent with several previous studies (e.g.: Itterly et al., 2016; Tanaka et al., 2014). Overall, the difference between the wet/dry seasons and the results presented in section 4.1 (with local observations) suggest that for the dry season, precipitation is controlled directly by large-meso scale circulation and local effects are less important. In contrast, the wet season suggests that local processes are more of the dominant factor in the night-time hours preceding the next days' diurnal rainfall.

5 Conclusions

In this paper, we present an alternative take on how daily precipitation is controlled by the night-time events over the Central Amazon. We break down our results based on season – wet and dry – and 2 modes of transition: non-raining evenings to non-raining days and non-raining evenings to raining days. The results suggest that during the wet season, local influences are the key driver of rainfall occurrence over our region of study. During the dry season, mesoscale-large scale factors are more important and dominate the development of the precipitation observed.

Moreover, precipitating cloud development is strongly associated with moisture availability, and boundary layer vertical motions or turbulence. We propose that during the wet season, when moisture levels observed are higher, cloud development is a direct effect of the local vertical motions. During the dry season, with moisture being less available and most of the incident solar radiation being converted to sensible heating, precipitating clouds are driven by large-meso scale circulation.

The results presented here suggest that during the wet season the diurnal precipitation is modulated mainly by the cloud coverage during overnight hours. Since cloud development is associated with vertical motion and moisture availability, and since during the wet season moisture is freely available, we speculate that the local scale nocturnal vertical motion is responsible for the cloud development. Therefore, the wet season NR-RR transition has a weaker upward vertical motion during the night (from 22 to 04 LT) and immediately following the sunrise (from 06 to 07 LT), reducing cloud formation during the first hours of the morning. This allows the surface to receive more solar energy, favoring instability. This is supported by the soil temperature and turbulent kinetic energy observations during the diurnal period. Since there is enough moisture available, we hypothesize that heating is transformed into latent heating, building convective cells that will precipitate later during the day. However, in the wet season NR-NR mode, nights with dominant shallow convection will reduce convection during the day, because the clouds formed during the night will reduce solar radiation at the surface

https://doi.org/10.5194/acp-2020-1098
Preprint. Discussion started: 22 October 2020

during the first hours of the day. During the wet season, a clear distinction during the night is observed between the NR-NR and NR-RR days, but for the dry season no significant signal is observed. This indicates that the local processes are not the key feature controlling the transition from shallow convection to rainfall between June and September. Previous studies (D'Almeida et al., 2007; Khanna et al., 2018; Lawrence and Vandecar, 2014) show that contrasts in land occupation (e.g.: forest and pasture, forest and deforested areas) have more impact on atmospheric and hydrological properties – PBL development, precipitation etc. during the dry season. These studies were performed measuring surface and atmospheric properties over different surfaces, showing that land occupation contrasts cause local circulations that can trigger convection and rainfall more often in the dry season. Here, we do not verify such land occupation contrasts, since all of our data was obtained over the same site (T3), and the site and its surrounding did not suffer any deforestation or change in its surface coverage over the 2 year period of our analysis.

The PBL analysis indicates that thermal turbulence does not play a major role on cloud formation during the dry season – there are no distinguishable differences between the NR-NR and the NR-RR transitions. Alternatively, the distinction between the transitions are clear during the wet season – both the turbulent kinetic energy and PBL heights have different values between raining and non-raining modes. TKE observations are corroborated by the soil temperature measurements, showing a connection between seasonal and rain-induced temperature differences and TKE observed.

In addition, the satellite data analysis shows that during the dry season precipitation is observed at T3 during days where cloud activity is seen throughout all its surroundings during the overnight hours, indicating a large-meso scale modulation in the convection during this season. There is a clear difference in the PDFs and CDFs between the raining modes. However, wet season brightness temperatures distributions are similar for NR-NR and NR-RR transitions. Statistically significant differences between NR-NR and NR-RR modes during the wet season are less frequent than those observed in the wet season, indicating that rainfall modulation during the wet season is less affected by the large-scale cloud background.

In summary, these results imply that models and parameterizations must consider different formulations based on the seasonal cycle to correctly resolve the precipitating convection over central Amazon. A convective parameterization scheme using only local or small-scale interactions will give poor results during the dry season. On the other hand, larger mass-flux convergence approaches will not perform well during the wet season, triggering precipitation at wrong times or quantifying it erroneously. Parameterizations schemes must consider seasonal differences in their formulation, and as already pointed out in several studies (D'Andrea et al., 2014; Gentine et al., 2013 and references therein), unified PBL/shallow convection/deep convection parametrization schemes present the better option to correct representation of the rainfall diurnal cycle.

Data availability

All ARM datasets used for this study can be downloaded at http://www.arm.gov and are associated with several "value added" product streams.

Author contributions

Thiago Biscaro: formal analysis, investigation, writing – original draft preparation, data curation. Luiz Machado: funding acquisition, conceptualization, writing – review and editing. Scott Giangrande and Michael Jensen: data curation, writing – review and editing.

Competing interests.

The authors declare that they have no conflict of interest.

https://doi.org/10.5194/acp-2020-1098
Preprint. Discussion started: 22 October 2020

Atmospheric Chemistry and Physics Discussions

Acknowledgements

We acknowledge FAPESP (São Paulo Research Foundation) projects 2009/15235-8 and 2015/14497-0. This paper has been authored by employees of Brookhaven Science Associates, LLC, under contract no DE-SC0012704 with the U.S. Department of Energy (DOE). The publisher by accepting the paper for publication acknowledges that the United States Government retains a nonexclusive, paid-up, irrevocable, worldwide license to publish or reproduce the published form of this paper, or allow others to do so, for United States Government purposes. We also acknowledge the Atmospheric Radiation Measurement (ARM) Climate Research Facility, a user facility of the U.S. DOE, Office of Science, sponsored by the Office of Biological and Environmental Research, and support from the ASR program of that office. We would like to thank SIPAM for providing the S-Band radar data. The manuscript was greatly improved by suggestions from David R. Fitzjarrald (Atmospheric Sciences Research Center, UAlbany, SUNY).

References

Ackerman, T. P. and Stokes, G. M.: The Atmospheric Radiation Measurement Program, *Physics Today*, 56(1), 38–44, doi:10.1063/1.1554135, 2003.

Anber, U., P. Gentine, S. G. Wang, and A. H. Sobel: Fog and rain in the Amazon, *Proc. Natl. Acad. Sci. U.S.A.*, **112**(37), 11,473– 11,477, 2015.

Atmospheric Radiation Measurement (ARM): Climate Research Facility: Balloon-Borne Sounding System (SONDE), 3.21297 S 60.5981 W: ARM Mobile Facility (MAO) Manacapuru, Amazonas, Brazil; AMF1 (M1), compiled by: Holdridge, D., Kyrouac, J., and Coulter, R., Atmospheric Radiation Measurement (ARM) Climate Research Facility Data Archive, Oak Ridge, Tennessee, USA, Data set accessed at 2018-07-01 https://doi.org/10.5439/1025284, 1993.

Atmospheric Radiation Measurement (ARM): Climate Research Facility: Radiative Flux Analysis (RADFLUX1LONG), 2014-01-01 to 2015-12-31, ARM Mobile Facility (MAO) Manacapuru, Amazonas, Brazil; AMF1 (M1), compiled by: Long, C., Gaustad, K., and Riihimaki, L.: Atmospheric Radiation Measurement (ARM) Climate Research Facility Data Archive: Oak Ridge, Tennessee, USA, Data set accessed 2018-07-01 at https://doi.org/10.5439/1157585, 2013.

Atmospheric Radiation Measurement (ARM) user facility: Ceilometer (CEILPBLHT). 2014-01-01 to 2015-12-31, ARM Mobile Facility (MAO) Manacapuru, Amazonas, Brazil; AMF1 (M1). Compiled by B. Ermold and V. Morris. ARM Data Center. Data set accessed 2018-07-01 at http://dx.doi.org/ 10.5439/1095593, 2013.

Atmospheric Radiation Measurement (ARM) user facility: Surface Energy Balance System (SEBS). 2014-01-01 to 2015-12-31, ARM Mobile Facility (MAO) Manacapuru, Amazonas, Brazil; AMF1 (M1). Compiled by D. Cook and R. Sullivan. ARM Data Center. Data set accessed 2018-07-01 at http://dx.doi.org/10.5439/1025274, 2013.

Atmospheric Radiation Measurement (ARM) user facility: W-band Cloud Radar Active Remote Sensing of Cloud (ARSCLWACR1KOLLIAS). 2014-01-01 to 2015-12-31, ARM Mobile Facility (MAO) Manacapuru, Amazonas, Brazil; AMF1 (M1). Compiled by K. Johnson and S. Giangrande. ARM Data Center. Data set accessed 2018-07-01 at http://dx.doi.org/ 10.5439/1097547, 2014.

Bechtold, P., Chaboureau, J.-P., Beljaars, A. C. M., Betts, A. K., Köhler, M., Miller, M. and Redelsperger, J.-L.: The simulationof the diurnal cycle of convective precipitation over land in a global model, *Quarterly Journal of the Royal Meteorological Society*, 130(604), 3119–3137, doi:10.1256/qj.03.103Betts, A. K. and Jakob, C. (2002). Evaluation of the diurnal cycle of precipitation, surface thermodynamics, and surface fluxes in the ECMWF model using LBA data, *Journal of Geophysical Research*, 107(D20), 8045, doi:10.1029/2001JD000427, 2004.

Betts, A. K., Fuentes, J. D., Garstang, M. and Ball, J. H.: Surface diurnal cycle and boundary layer structure over Rondonia during the rainy season, *Journal of Geophysical Research*, 107, 8065, doi:10.1029/2001JD000356, 2002.

https://doi.org/10.5194/acp-2020-1098
Preprint. Discussion started: 22 October 2020

Betts, A.K., Ball, J., Barr, A, Black, T. A., McCaughey, J. H. and P. Viterbo, P.: Assessing land-surface-atmosphere coupling in the ERA-40 reanalysis with boreal forest data. *Agricultural and Forest Meteorology*, 140, 355-382, doi:10.1016/j.agrformet.2006.08.009, 2006.

Betts, A. K., Fisch, G., Von Randow, C., Silva Dias, M. A. F., Cohen, J. C. P., Da Silva, R. and Fitzjarrald, D. R.: The Amazonian Boundary Layer and Mesoscale Circulations, in Amazonia and Global Change, 2013.

Carneiro, R.G. (2018). Erosão da camada limite noturna e suas implicações no crescimento da camada limite convectiva na região central da Amazônia (experimento GOAMAZON 2014/15). Doctoral thesis, Instituto Nacional de Pesquisas Espaciais, Brazil. 152p. (http://urlib.net/sid.inpe.br/mtc-m21b/2018/01.18.01.59), 2018.

Carneiro, R. G., Fisch, G., Borges, C. K., and Henkes, A.: Erosion of the nocturnal boundary layer in the central Amazon during the dry season. Acta Amazonica, 50(1), 80-89. Epub November 25, 2019.https://doi.org/10.1590/1809-4392201804453, 2020.

Clothiaux, E. E., Ackerman, T. P., Mace, G. G., Moran, K. P., Marchand, R. T., Miller, M. A. and Martner, B. E.: Objective Determination of Cloud Heights and Radar Reflectivities Using a Combination of Active Remote Sensors at the ARM CART Sites, *Journal of Applied Meteorology*, 39(5), 645–665, doi:10.1175/1520-0450(2000)039<0645:ODOCHA>2.0.CO;2, 2000.

Cohen, J.C.P., Fitzjarrald, D.R., D'Oliveira, F.A.F., Saraiva, I., Barbosa, I.R.D.S., Gandu, A.W. and Kuhn, P.A.: Radar-observed spatial and temporal rainfall variability near the Tapajós-Amazon confluence. *Revista Brasileira de Meteorologia*, 29(SPE), pp.23-30, 2014

Costa, S. M. S., Negri, R. G., Ferreira, N. J., Schmit, T. J., Arai, N., Flauber, W., Ceballos, J., Vila, D., Rodrigues, J., Machado, L. A., Pereira, S., Bottino, M. J., Sismanoglu, R. A. and Langden, P.: A Successful Practical Experience with Dedicated Geostationary Operational Environmental Satellites GOES-10 and -12 Supporting Brazil, *Bulletin of the American Meteorological Society*, 99(1), 33–47, doi:10.1175/BAMS-D-16-0029.1, 2018

Dai, A.: Precipitation characteristics in eighteen coupled climate models, *Journal of Climate*, 19(18), 4605–4630, doi:10.1175/JCLI3884.1, 2006.

D'Almeida, C., Vörösmarty, C. J., Hurtt, G. C., Marengo, J. A., Dingman, S. L., & Keim, B. D.: The effects of deforestation on the hydrological cycle in Amazonia: a review on scale and resolution. *International Journal of Climatology*, 27(5), 633–647. https://doi.org/10.1002/joc.1475, 2007.

D'Andrea, F., Gentine, P., Betts, A. K. and Lintner, B. R.: Triggering deep convection with a probabilistic plume model. *Journal of Atmospheric Sciences*, 71, 3881–3901, https://doi.org/10.1175/JAS-D-13-0340.1, 2014.

Fisch, G., Tota, J., Machado, L.A.T., Dias, M.S., Lyra, R.D.F., Nobre, C.A., Dolman, A.J. and Gash, J.H.C.: The convective boundary layer over pasture and forest in Amazonia. Theoretical and Applied Climatology, 78(1-3), pp.47-59, 2004.

Fitzjarrald, D. R., Sakai, R. K., Moraes, O. L. L., Cosme de Oliveira, R., Acevedo, O. C., Czikowsky, M. J., and Beldini, T.: Spatial and temporal rainfall variability near the Amazon-Tapajós confluence, J. Geophys. Res., 113, G00B11, doi:10.1029/2007JG000596, 2008.

Fu, R. and Li, W.: The influence of the land surface on the transition from dry to wet season in Amazonia, *Theoretical and Applied Climatology*, 78(1–3), 97–110, doi:10.1007/s00704-004-0046-7, 2004.

Garstang, M., Ulanski, S., Greco, S., Scala, J., Swap, R., Fitzjarrald, D., Martin, D., Browell, E., Shipman, M., Connors, V. and Harriss, R.: The Amazon boundary-layer experiment (ABLE 2B): A meteorological perspective. Bulletin of the American Meteorological Society, 71(1), pp.19-32, 1990.

Gentine, P., Betts, A. K., Lintner, B. R., Findell, K. L., van Heerwaarden, C. C. and D'Andrea, F.: A Probabilistic Bulk Model of Coupled Mixed Layer and Convection. Part II: Shallow Convection Case, *Journal of Atmospheric Sciences*, 70(6), 1557–1576, doi:10.1175/JAS-D-12-0146.1, 2013.

490 Ghate, V. P. and Kollias, P.: On the Controls of Daytime Precipitation in the Amazonian Dry Season, *Journal of Hydrometeorology*, 17(12), 3079–3097, doi:10.1175/JHM-D-16-0101.1, 2016.

Giangrande, S. E., Feng, Z., Jensen, M. P., Comstock, J. M., Johnson, K. L., Toto, T., Wang, M., Burleyson, C., Bharadwaj, N., Mei, F., Machado, L. A. T., Manzi, A. O., Xie, S., Tang, S., Silva Dias, M. A. F., de Souza, R. A. F., Schumacher, C. and Martin, S. T.: Cloud characteristics, thermodynamic controls and radiative impacts during the Observations and Modeling of
495 the Green Ocean Amazon (GoAmazon2014/5) experiment, *Atmospheric Chemistry and Physics*, 17(23), 14519–14541, doi:10.5194/acp-17-14519-2017, 2017.

Giangrande, S. E., Wang, D., and Mechem, D. B.: Cloud regimes over the Amazon basin: perspectives from the GoAmazon2014/5 campaign. *Atmospheric Chemistry and Physics Discussions*, 2020, 1-36, https://www.atmos-chem-phys-discuss.net/acp-2020-67/, 2020.

500 Harriss, R.C., Wofsy, S.C., Garstang, M., Browell, E.V., Molion, L.C.B., McNeal, R.J., Hoell, J.M., Bendura, R.J., Beck, S.M., Navarro, R.L. and Riley, J.T.: The Amazon boundary layer experiment (ABLE 2A): Dry season 1985. Journal of Geophysical Research: Atmospheres, 93(D2), pp.1351-1360, 1988.

Houze, R. A.: 100 years of research on mesoscale convective systems. *Meteorological Monographs*, 59, 17.1– 17.54. https://doi.org/10.1175/AMSMONOGRAPHS-D-18-0001.1, 2018.

505 Huntingford, C., Harris, P. P., Gedney, N., Cox, P. M., Betts, R. A., Marengo, J. A. and Gash, J. H. C. (2004). Using a GCM analogue model to investigate the potential for Amazonian forest dieback, *Theoretical and Applied Climatology*, 78(1–3), 177–185, doi:10.1007/s00704-004-0051-x, 2004.

Hwang, Y.-T. and Frierson, D. M. W.: Link between the double-Intertropical Convergence Zone problem and cloud biases over the Southern Ocean, *Proceedings of the National Academy of Sciences of the United States of America*, 110(13), 4935–
510 4940, doi:10.1073/pnas.1213302110, 2013.

Itterly, K. F., Taylor, P. C., Dodson, J. B. and Tawfik, A. B.: On the sensitivity of the diurnal cycle in the Amazon to convective intensity, *Journal of Geophysical Research*: *Atmospheres*, 121(14), 8186–8208, doi:10.1002/2016JD025039, 2016.

Jacobson, M.Z.: Fundamentals of Atmospheric Modelling. 2nd Edition (Cambridge University Press, Cambridge, UK), 2015.

515 Jensen, M. P., Toto, T., Troyan, D., Ciesielski, P. E., Holdridge, D., Kyrouac, J., Schatz, J., Zhang, Y., and Xie, S.: The Mid-latitude Continental Convective Clouds Experiment (MC3E) sounding network: operations, processing and analysis, *Atmospheric Measurement Techniques*, 8, 421–434, https://doi.org/10.5194/amt-8-421-2015, 2015.

Jiménez-Muñoz, J.C.; Mattar, C.; Barichivich, J.; Santamaría-Artigas, A.; Takahashi, K.; Malhi, Y.; Sobrino, J.A.; Schrier, G.V.D. Record-breaking warming and extreme drought in the Amazon rainforest during the course of El Niño 2015–
520 2016. *Sci. Rep. 6*, 33130, doi: 10.1038/srep33130, 2016.

Jones, A.R.; Brunsell, N.A.: Energy balance partitioning and net radiation controls on soil moisture-precipitation feedbacks, *Earth Interact*, 13, 1–25, 2009.

Khairoutdinov, M. and Randall, D.: High-Resolution Simulation of Shallow-to-Deep Convection Transition over Land, *Journal of Atmospheric Sciences*, 63(12), 3421–3436, doi:10.1175/JAS3810.1, 2006.

525 Khanna, J., Medvigy, D., Fisch, G., & de Araújo Tiburtino Neves, T. T.: Regional Hydroclimatic Variability Due To Contemporary Deforestation in Southern Amazonia and Associated Boundary Layer Characteristics. *Journal of Geophysical Research: Atmospheres*, 123(8), 3993–4014. https://doi.org/10.1002/2017jd027888, 2018.

Lawrence, D., & Vandecar, K.: Effects of tropical deforestation on climate and agriculture. *Nature Climate Change*, 5(1), 27–36. https://doi.org/10.1038/nclimate2430, 2014.

530 Machado, L. A. T.: The Amazon Energy Budget Using the ABLE-2B and FluAmazon Data, *Journal of Atmospheric Sciences*, 57(18), 3131–3144, doi:10.1175/1520-0469(2000)057<3131:TAEBUT>2.0.CO;2, 2000.

https://doi.org/10.5194/acp-2020-1098
Preprint. Discussion started: 22 October 2020

Machado, L. A. T., Laurent, H. and Lima, A. A.: Diurnal march of the convection observed during TRMM-WETAMC/LBA, *Journal of Geophysical Research*, 107(D20), 8064, doi:10.1029/2001JD000338, 2002.

Machado, L. A. T., Silva Dias, M. A. F., Morales, C., Fisch, G., Vila, D., Albrecht, R., Goodman, S. J., Calheiros, A. J. P., Biscaro, T., Kummerow, C., Cohen, J., Fitzjarrald, D., Nascimento, E. L., Sakamoto, M. S., Cunningham, C., Chaboureau, J.-P., Petersen, W. A., Adams, D. K., Baldini, L., Angelis, C. F., Sapucci, L. F., Salio, P., Barbosa, H. M. J., Landulfo, E., Souza, R. A. F., Blakeslee, R. J., Bailey, J., Freitas, S., Lima, W. F. A., Tokay, A., Machado, L. A. T., Dias, M. A. F. S., Morales, C., Fisch, G., Vila, D., Albrecht, R., Goodman, S. J., Calheiros, A. J. P., Biscaro, T., Kummerow, C., Cohen, J., Fitzjarrald, D., Nascimento, E. L., Sakamoto, M. S., Cunningham, C., Chaboureau, J.-P., Petersen, W. A., Adams, D. K., Baldini, L., Angelis, C. F., Sapucci, L. F., Salio, P., Barbosa, H. M. J., Landulfo, E., Souza, R. A. F., Blakeslee, R. J., Bailey, J., Freitas, S., Lima, W. F. A. and Tokay, A. (2014). The CHUVA Project: How Does Convection Vary across Brazil?, *Bulletin of the American Meteorological Society*, 95(9), 1365–1380, doi:10.1175/BAMS-D-13-00084.1, 2014.

Machado, L. A. T., Calheiros, A. J. P., Biscaro, T., Giangrande, S., Silva Dias, M. A. F., Cecchini, M. A., Albrecht, R., Andreae, M. O., Araujo, W. F., Artaxo, P., Borrmann, S., Braga, R., Burleyson, C., Eichholz, C. W., Fan, J., Feng, Z., Fisch, G. F., Jensen, M. P., Martin, S. T., Pöschl, U., Pöhlker, C., Pöhlker, M. L., Ribaud, J.-F., Rosenfeld, D., Saraiva, J. M. B., Schumacher, C., Thalman, R., Walter, D., and Wendisch, M.: Overview: Precipitation characteristics and sensitivities to environmental conditions during GoAmazon2014/5 and ACRIDICON-CHUVA, *Atmospheric Chemistry and Physics*, 18, 6461-6482, https://doi.org/10.5194/acp-18-6461-2018, 2018.

Martin, C.L., Fitzjarrald, D., Garstang, M., Oliveira, A.P., Greco, S. and Browell, E.: Structure and growth of the mixing layer over the Amazonian rain forest. Journal of Geophysical Research: Atmospheres, 93(D2), pp.1361-1375, 1988.

Martin, S. T., Artaxo, P., Machado, L., Manzi, A. O., Souza, R. A. F., Schumacher, C., Wang, J., Biscaro, T., Brito, J., Calheiros, A., Jardine, K., Medeiros, A., Portela, B., de Sá, S. S., Adachi, K., Aiken, A. C., Albrecht, R., Alexander, L., Andreae, M. O., Barbosa, H. M. J., Buseck, P., Chand, D., Comstock, J. M., Day, D. A., Dubey, M., Fan, J., Fast, J., Fisch, G., Fortner, E., Giangrande, S., Gilles, M., Goldstein, A. H., Guenther, A., Hubbe, J., Jensen, M., Jimenez, J. L., Keutsch, F. N., Kim, S., Kuang, C., Laskin, A., McKinney, K., Mei, F., Miller, M., Nascimento, R., Pauliquevis, T., Pekour, M., Peres, J., Petäjä, T., Pöhlker, C., Pöschl, U., Rizzo, L., Schmid, B., Shilling, J. E., Silva Dias, M. A., Smith, J. N., Tomlinson, J. M., Tóta, J., Wendisch, M., Martin, S. T., Artaxo, P., Machado, L., Manzi, A. O., Souza, R. A. F., Schumacher, C., Wang, J., Biscaro, T., Brito, J., Calheiros, A., Jardine, K., Medeiros, A., Portela, B., Sá, S. S. de, Adachi, K., Aiken, A. C., Albrecht, R., Alexander, L., Andreae, M. O., Barbosa, H. M. J., Buseck, P., Chand, D., Comstock, J. M., Day, D. A., Dubey, M., Fan, J., Fast, J., Fisch, G., Fortner, E., Giangrande, S., Gilles, M., Goldstein, A. H., Guenther, A., Hubbe, J., Jensen, M., Jimenez, J. L., Keutsch, F. N., Kim, S., Kuang, C., Laskin, A., McKinney, K., et al.: The Green Ocean Amazon Experiment (GoAmazon2014/5) Observes Pollution Affecting Gases, Aerosols, Clouds, and Rainfall over the Rain Forest, *Bulletin of the American Meteorological Society*, BAMS-D-15-00221.1, doi:10.1175/BAMS-D-15-00221.1, 2016.

Mather, J. H. and Voyles, J. W.: The AM Climate Resarch Facility: A Reviw of Sructire and Capabilities. *Bulletin of the American Meteorological Society*, 94(3), 377-392, doi: 10.1175/BAMS-D-11-00218.11, 2013.

Miller, M. A., Nitschke, K., Ackerman, T. P., Ferell, W. R., Hickmon, N. and Ivery, M.: The ARM Mobile Facilities. *Meteorological Monographs*, No. 57, Amer. Meteor. Soc., doi:10.1175/AMSMONOGPHS-D-15-0051.1, 2016.

de Oliveira, A.P. and Fitzjarrald, D.R.: The Amazon river breeze and the local boundary layer: I. Observations. Boundary-Layer Meteorology 63, 141–162. https://doi.org/10.1007/BF00705380

Oliveira, R., Maggioni, V., Vila, D. and Morales, C.: Characteristics and diurnal cycle of GPM rainfall estimates over the Central Amazon region, *Remote Sensing*, 8(7), doi:10.3390/rs8070544, 2016.

Rickenbach, T. M., Ferreira, R. N., Halverson, J. B., Herdies, D. L. and Silva Dias, M. A. F.: Modulation of convection in the southwestern Amazon basin by extratropical stationary fronts, *Journal of Geophysical Research*, 107(D20), 8040, doi:10.1029/2000JD000263, 2002.

https://doi.org/10.5194/acp-2020-1098
Preprint. Discussion started: 22 October 2020

Atmospheric Chemistry and Physics Discussions

575 Sato, T., Miura, H., Satoh, M., Takayabu, Y. N. and Wang, Y.: Diurnal cycle of precipitation in the tropics simulated in a global cloud-resolving model, *Journal of Climate*, 22(18), 4809–4826, doi:10.1175/2009JCLI2890.1

Schiro, K. A. and Neelin, J. D.: Tropical continental downdraft characteristics: mesoscale systems versus unorganized convection, *Atmospheric Chemistry and Physics*, 18, 1997-2010, https://doi.org/10.5194/acp-18-1997-2018, 2018.

Silva Dias, M. A. F., Rutledge, S., Kabat, P., Silva Dias, P. L., Nobre, C., Fisch, G., Dolman, A. J., Zipser, E., Garstang, M.,
580 Manzi, A. O., Fuentes, J. D., Rocha, H. R., Marengo, J., Plana-Fattori, A., Sá, L. D. A., Alvalá, R. . C. S., Andreae, M. O., Artaxo, P., Gielow, R. and Gatti, L.: Cloud and rain processes in a biosphere-atmosphere interaction context in the Amazon Region, *Journal of Geophysical Research*, 107(D20), 8072, doi:10.1029/2001JD000335, 2002.

Stratton, R. A. and Stirling, A. J.: Improving the diurnal cycle of convection in GCMs, Q. J. R. Meteorol. Soc., 138(666), 1121–1134, doi:10.1002/qj.991, 2012.

585 Tanaka, L. M. D. S., Satyamurty, P. and Machado, L. A. T.: Diurnal variation of precipitation in central Amazon Basin, *International Journal of Climatology*, 34(13), 3574–3584, doi:10.1002/joc.3929, 2014.

Wendisch, M., Pöschl, U., Andreae, M. O., Machado, L. A. T., Albrecht, R., Schlager, H., Rosenfeld, D., Martin, S. T., Abdelmonem, A., Afchine, A., Araùjo, A., Artaxo, P., Aufmhoff, H., Barbosa, H. M. J., Borrmann, S., Braga, R., Buchholz, B., Cecchini, M. A., Costa, A., Curtius, J., Dollner, M., Dorf, M., Dreiling, V., Ebert, V., Ehrlich, A., Ewald, F., Fisch, G.,
590 Fix, A., Frank, F., Fütterer, D., Heckl, C., Heidelberg, F., Hüneke, T., Jäkel, E., Järvinen, E., Jurkat, T., Kanter, S., Kästner, U., Kenntner, M., Kesselmeier, J., Klimach, T., Knecht, M., Kohl, R., Kölling, T., Krämer, M., Krüger, M., Krisna, T. C., Lavric, J. V., Longo, K., Mahnke, C., Manzi, A. O., Mayer, B., Mertes, S., Minikin, A., Molleker, S., Münch, S., Nillius, B., Pfeilsticker, K., Pöhlker, C., Roiger, A., Rose, D., Rosenow, D., Sauer, D., Schnaiter, M., Schneider, J., Schulz, C., de Souza, R. A. F., Spanu, A., Stock, P., Vila, D., Voigt, C., Walser, A., Walter, D., Weigel, R., Weinzierl, B., Werner, F.,
595 Yamasoe, M. A., Ziereis, H., Zinner, T., Zöger, M., Wendisch, M., Pöschl, U., Andreae, M. O., Machado, L. A. T., Albrecht, R., Schlager, H., Rosenfeld, D., Martin, S. T., Abdelmonem, A., Afchine, A., Araùjo, A., Artaxo, P., Aufmhoff, H., Barbosa, H. M. J., Borrmann, S., Braga, R., Buchholz, B., Cecchini, M. A., Costa, A., et al.: The ACRIDICON-CHUVA campaign: Studying tropical deep convective clouds and precipitation over Amazonia using the new German research aircraft HALO, *Bulletin of the American Meteorological Society*, BAMS-D-14-00255.1, doi:10.1175/BAMS-D-14-00255.1, 2016.

600 Wang, D., Giangrande, S. E., Bartholomew, M. J., Hardin, J., Feng, Z., Thalman, R., and Machado, L. A. T: The Green Ocean: precipitation insights from the GoAmazon2014/5 experiment, *Atmospheric Chemistry and Physics*, 18, 9121-9145, https://doi.org/10.5194/acp-18-9121-2018, 2018.

https://doi.org/10.5194/acp-2020-1098
Preprint. Discussion started: 22 October 2020

Atmospheric Chemistry and Physics Discussions

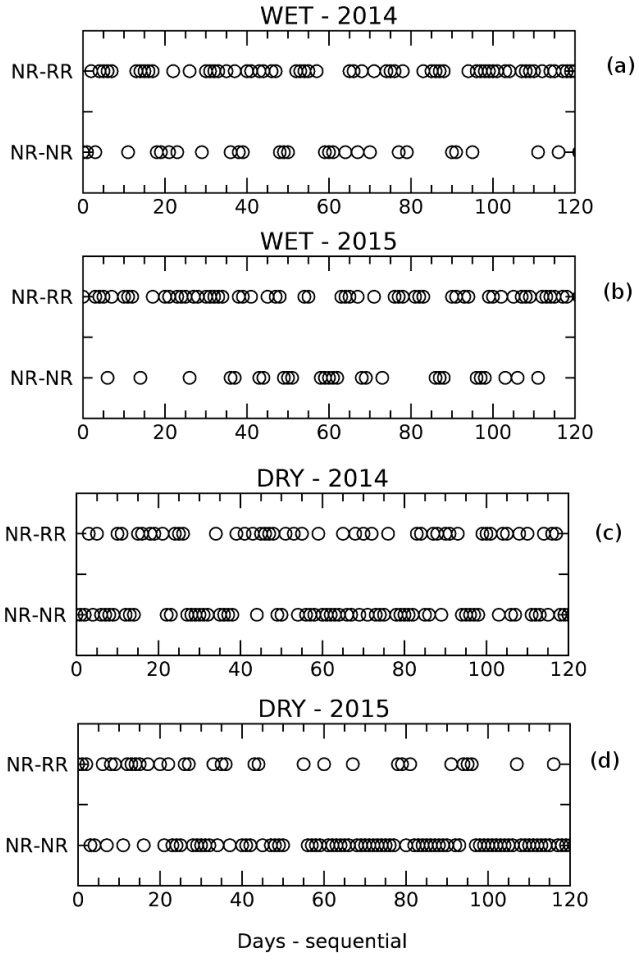

605

Figure 1: NR-NR and NR-RR cases distribution during the wet and dry seasons of 2014 and 2015. Day zero is defined as the January 1st for the wet season and June 1st for the dry season.

https://doi.org/10.5194/acp-2020-1098
Preprint. Discussion started: 22 October 2020

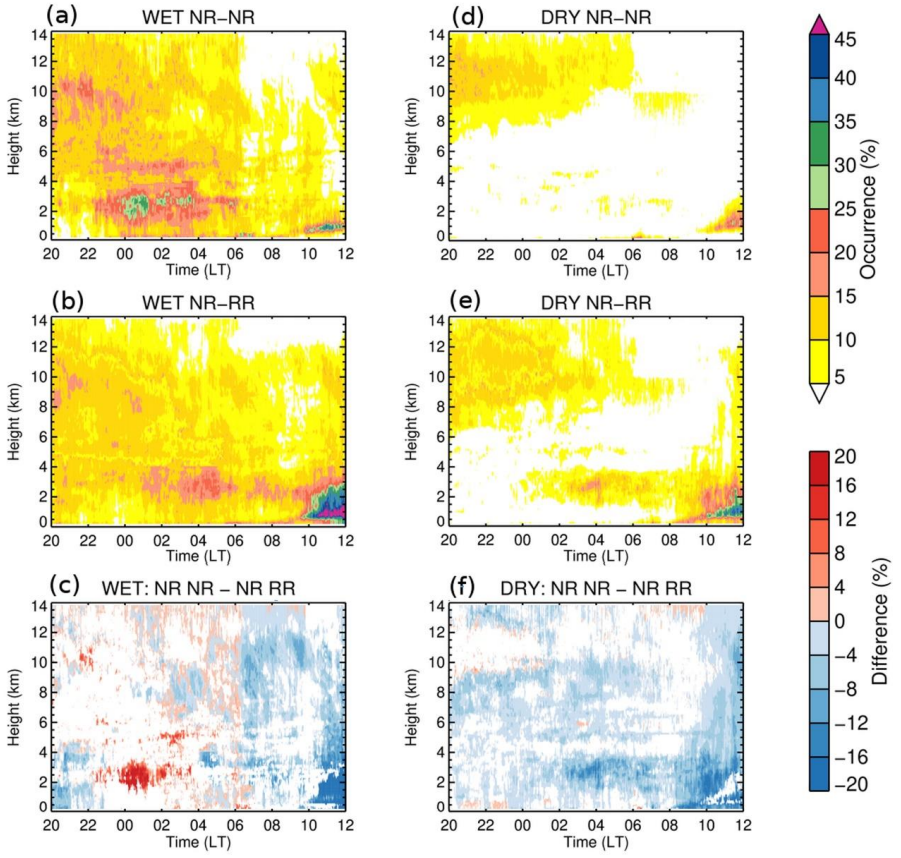

610

Figure 2: Cloud occurrence and absolute differences between non-raining and raining transitions, for wet and dry seasons. Sub-panel (a): wet-season NR-NR cloud fraction; (b) wet-season NR-RR cloud fraction; (c) wet-season cloud fraction difference between NR-NR and NR-RR modes; (d): dry-season NR-NR cloud fraction; (e) dry-season NR-RR cloud fraction; (f) dry-season cloud fraction difference between NR-NR and NR-RR modes. Non-significant differences (areas where differences and their 615 **standard deviations overlap) are marked in white in the bottom panels.**

https://doi.org/10.5194/acp-2020-1098
Preprint. Discussion started: 22 October 2020

Atmospheric Chemistry and Physics Discussions

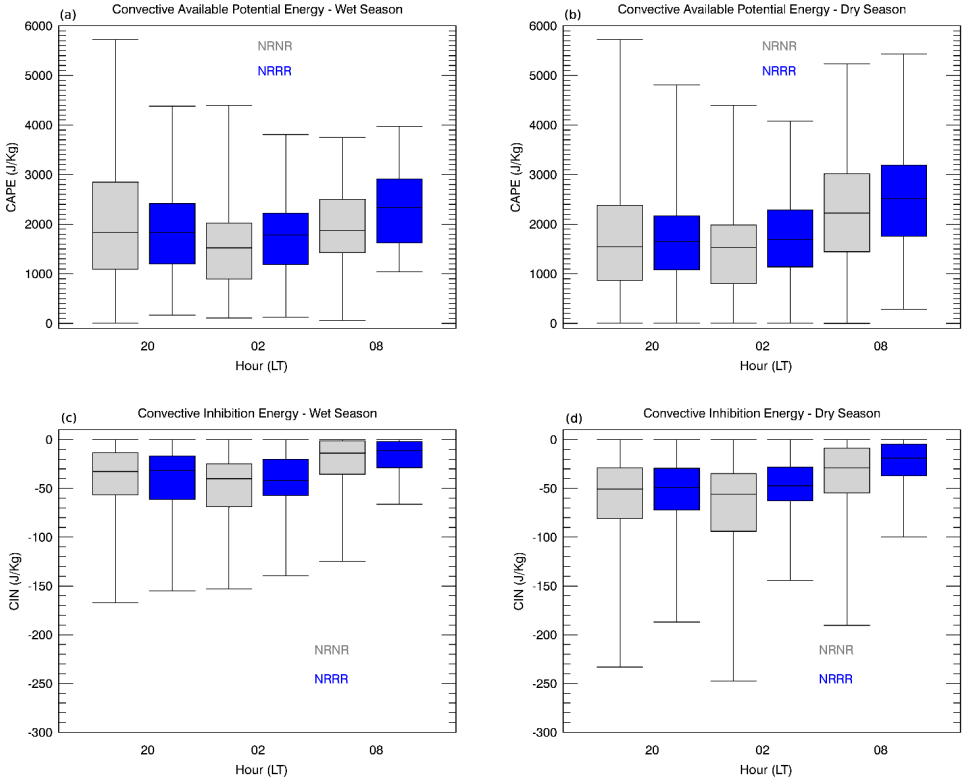

620 **Figure 3: CAPE and CIN statistics derived with the radiosondes during the nocturnal period at T3, for dry and wet seasons and NR-NR and NR-RR transitions. The boxes and whiskers represent the minimum (excluding possible outliers), the lower quartile, the median, the upper quartile, and the maximum (excluding possible outliers).**

https://doi.org/10.5194/acp-2020-1098
Preprint. Discussion started: 22 October 2020

Atmospheric Chemistry and Physics Discussions

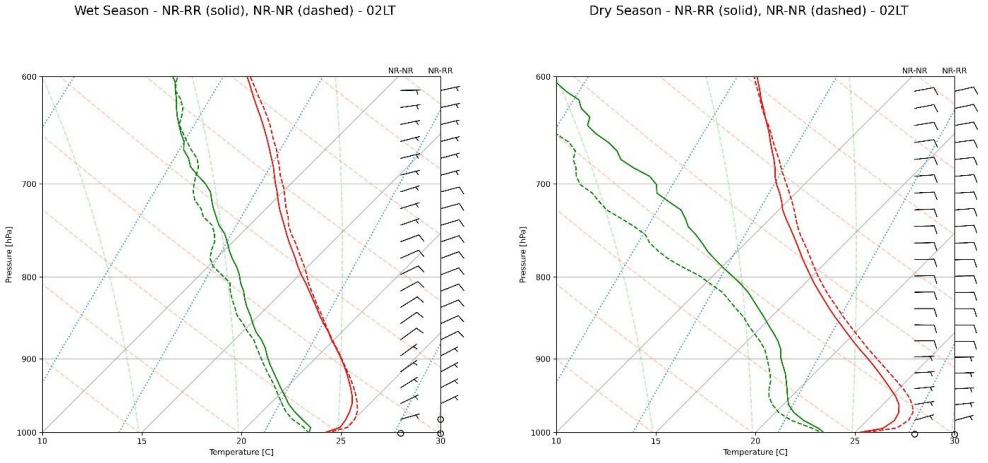

Figure 4: Composite 02 LT radiosondes launched at T3. Left panel shows the wet season and right panel shows the dry season. Solid lines are NR-RR data, and dashed lines are NR-NR data. The red line is dry temperature and green the dewpoint temperature.

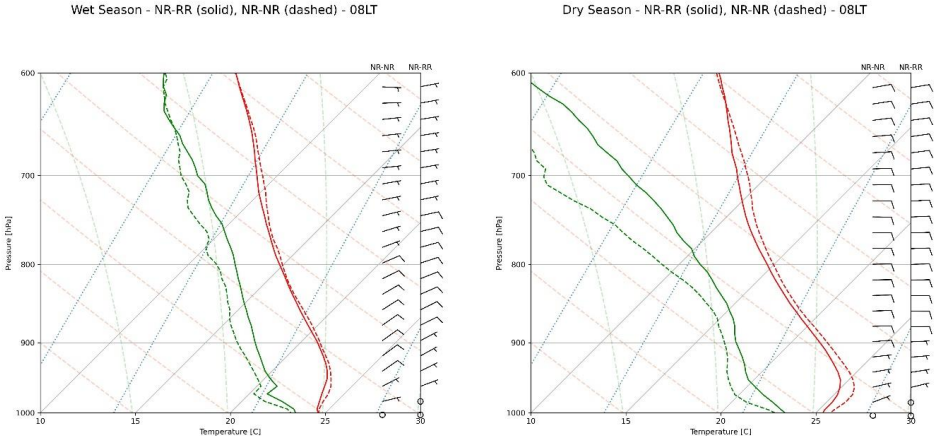

Figure 5: Same as Figure 4 but for the 08 LT radiosondes.

https://doi.org/10.5194/acp-2020-1098
Preprint. Discussion started: 22 October 2020

Atmospheric Chemistry and Physics Discussions

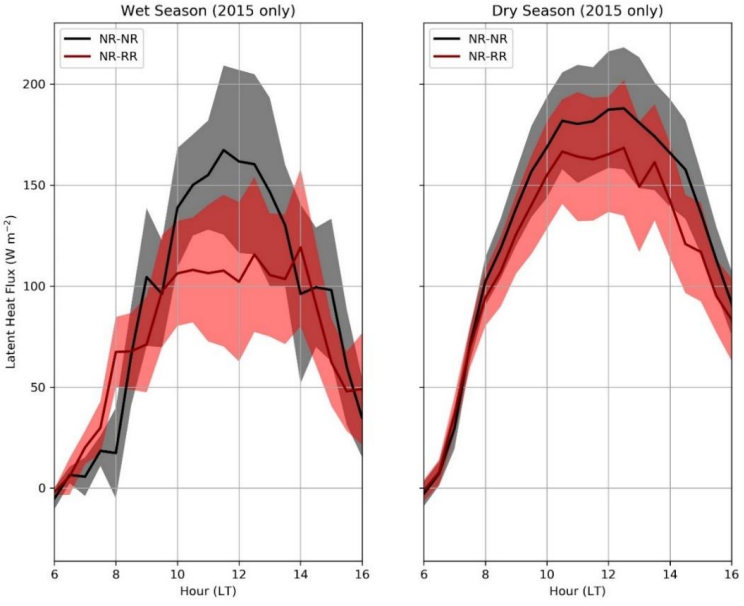

Figure 6: Mean (composite dataset) latent heat fluxes measured by ECOR, for dry and wet seasons and NR-NR and NR-RR transitions. Shaded areas represent one standard deviation.

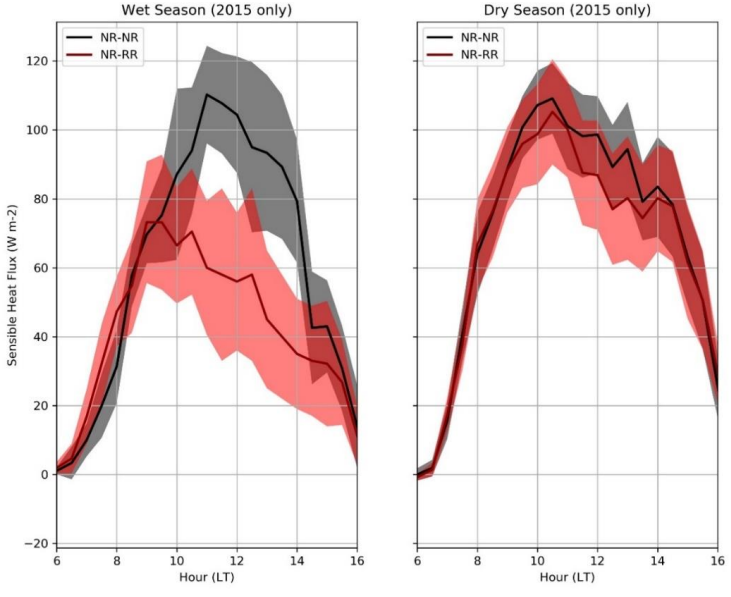

635

Figure 7: Mean (composite dataset) sensible heat fluxes measured by ECOR, for dry and wet seasons and NR-NR and NR-RR transitions. Shaded areas represent one standard deviation.

https://doi.org/10.5194/acp-2020-1098
Preprint. Discussion started: 22 October 2020

Atmospheric Chemistry and Physics Discussions

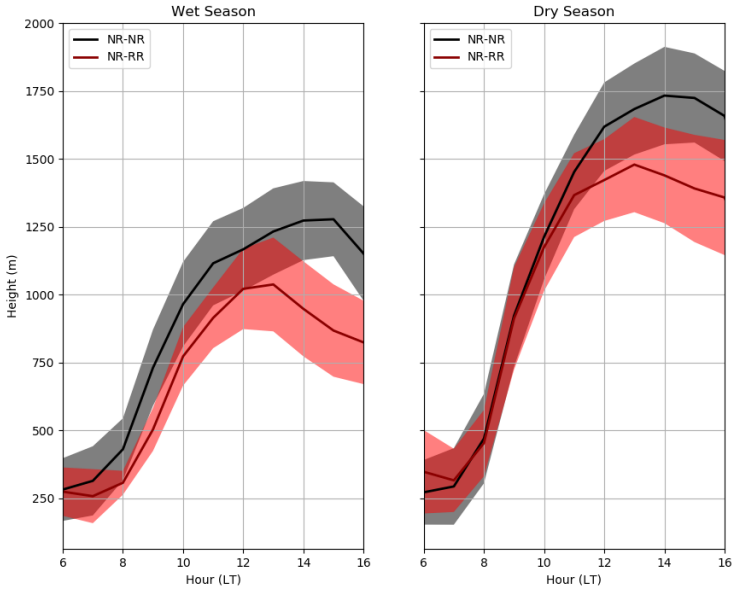

640 **Figure 8: Planetary Boundary Layer mean (composite dataset) height derived with the ceilometer, for dry and wet seasons and NR-NR and NR-RR transitions. Shaded areas represent one standard deviation.**

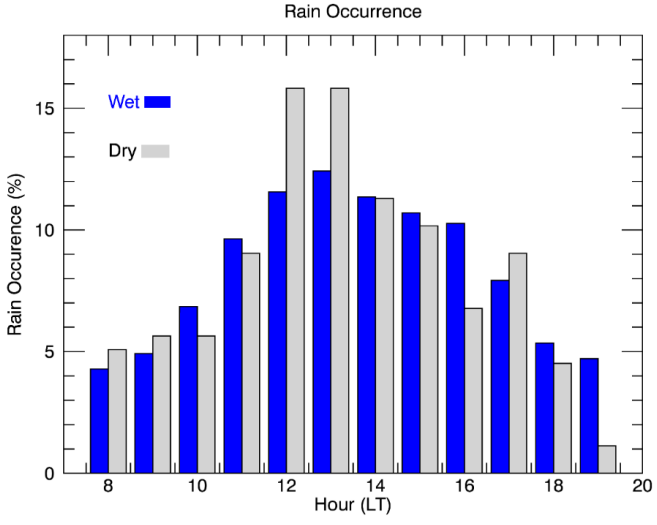

645 **Figure 9: Normalized hourly rainfall occurrence distribution observed over T3, for the wet and dry seasons (NR-RR days only).**

https://doi.org/10.5194/acp-2020-1098
Preprint. Discussion started: 22 October 2020

Atmospheric Chemistry and Physics Discussions

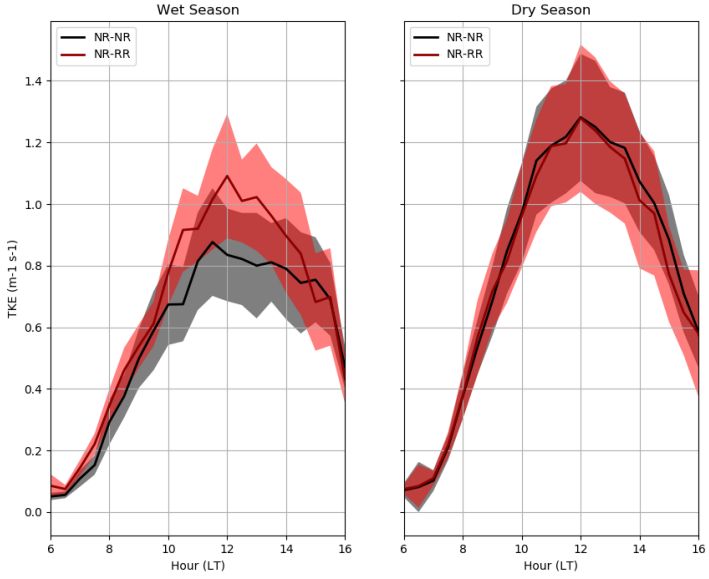

Figure 10: Mean (composite dataset) turbulent kinetic energy derived with the ECOR, for dry and wet seasons and NR-NR and NR-RR transitions. Shaded areas represent one standard deviation.

650

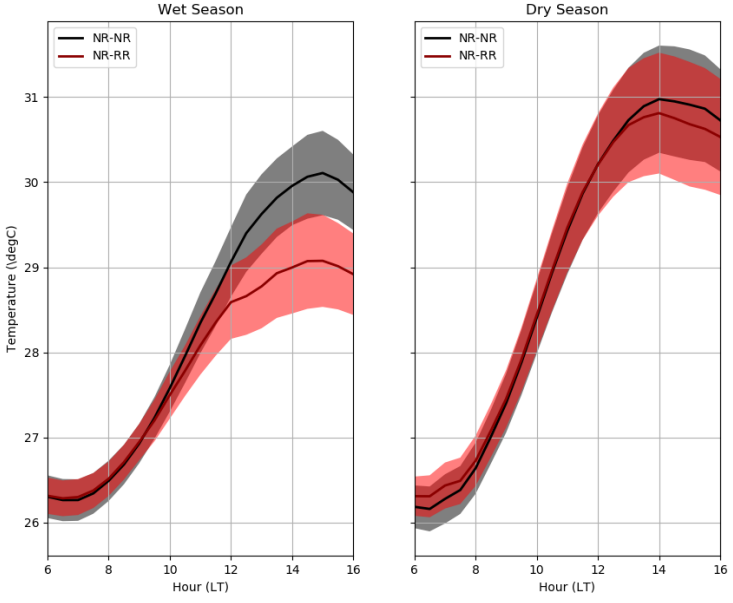

Figure 11: Mean (composite dataset) soil temperature as measured by SEBS, for dry and wet seasons and NR-NR and NR-RR transitions. Shaded areas represent one standard deviation.

https://doi.org/10.5194/acp-2020-1098
Preprint. Discussion started: 22 October 2020

Atmospheric Chemistry and Physics Discussions

655

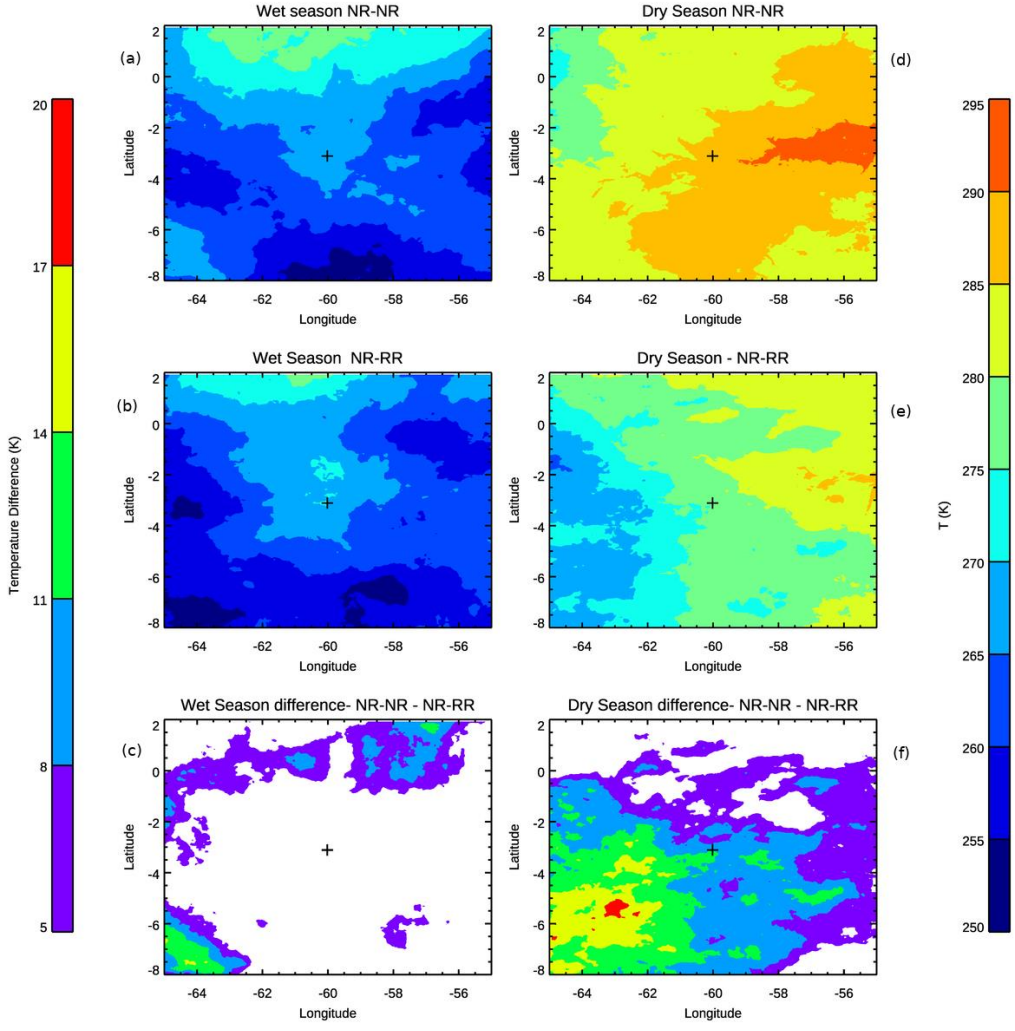

Figure 12: Mean GOES 10.4 µm brightness temperature fields and absolute differences from 20 LT to 08 LT, for dry and wet seasons and NR-NR and NR-RR transitions. The cross mark represents the T3 position. Non-significant differences (areas where differences and their standard deviations overlap) are marked in white.

660

https://doi.org/10.5194/acp-2020-1098
Preprint. Discussion started: 22 October 2020

Atmospheric Chemistry and Physics Discussions

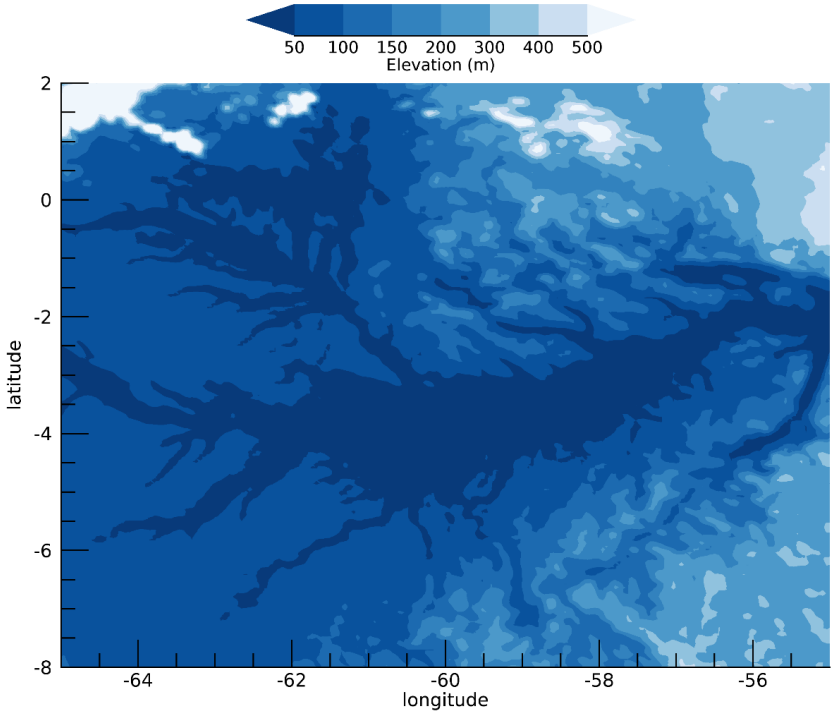

Figure 13: Terrain elevation for the large-mesoscale analysis domain.

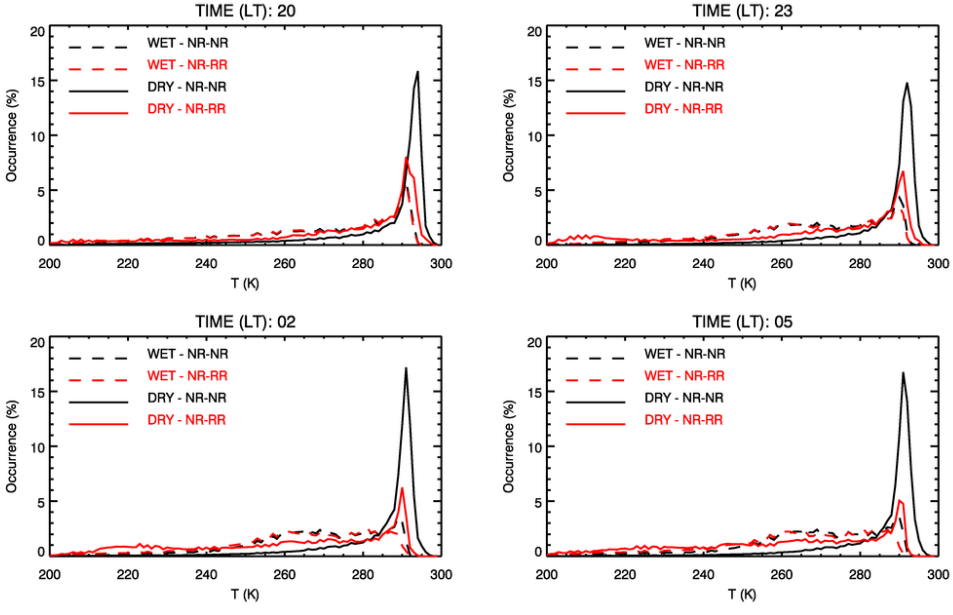

Figure 14: Probability distributions (grouped in 3h groups) of GOES 10.4 μm brightness temperatures, for dry and wet seasons and NR-NR and NR-RR transitions during the night-time period. Time at each panel is the start time (LT).

https://doi.org/10.5194/acp-2020-1098
Preprint. Discussion started: 22 October 2020

Atmospheric Chemistry and Physics Discussions

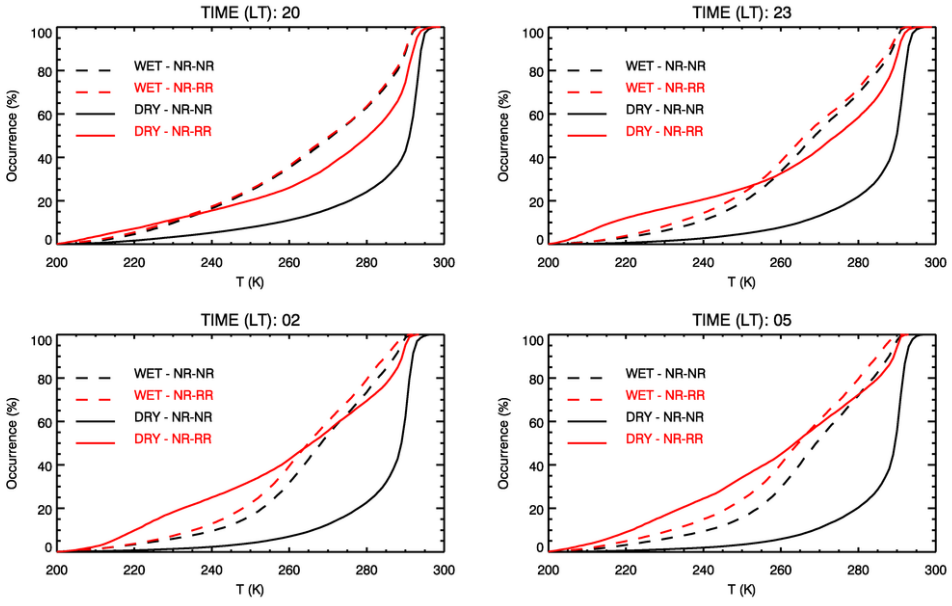

Figure 15: Cumulative distribution functions (grouped in 3h groups) of GOES 10.4 μm brightness temperatures, for dry and wet seasons and NR-NR and NR-RR transitions during the night-time period. Time at each panel is the start time (LT).